Journal of Integrative Neuroscience

J. Integr. Neurosci. **2026**; 25(8): 51000
https://doi.org/10.31083/JIN51000

Original Research

Sodium Rutin Alleviates Neuronal Apoptosis and Promotes Locomotor Recovery in Distractive Spinal Cord Injury via ErbB4 and ROS Signaling

Weishi Liang[1,2,†], Yeqiu Xu[1,2,†], Junrui Jonathan Hai[2,3], Duan Sun[1,2], Yihan Yang[1,2], Chen Wang[2], Peng Yin[1,2], Yajin Liao[4], Bo Han[2,5], Xianjun Qu[2,6,*], Yong Hai[1,2,*]

[1]Department of Orthopedic Surgery, Beijing Chaoyang Hospital, Capital Medical University, 100020 Beijing, China
[2]Joint Laboratory for Research & Treatment of Spinal Cord Injury in Spinal Deformity, Capital Medical University, 100069 Beijing, China
[3]Krieger School of Arts and Sciences, Johns Hopkins University, Baltimore, MD 21218, USA
[4]NHC Key Laboratory of Neurodegenerative diseases (University of South China), 421001 Hengyang, Hunan, China
[5]Department of Spinal Surgery, Beijing Jishuitan Hospital, Capital Medical University, 100035 Beijing, China
[6]Department of Pharmacology, School of Basic Medical Sciences, Capital Medical University, 100069 Beijing, China
*Correspondence: qxj@ccmu.edu.cn (Xianjun Qu); yong.hai@ccmu.edu.cn (Yong Hai)
[†]These authors contributed equally.
Academic Editor: Nuno A. Silva
Submitted: 13 February 2026 Revised: 6 April 2026 Accepted: 14 April 2026 Published: 13 August 2026

Abstract

Background: Distractive spinal cord injury (DSCI), a severe complication of spinal deformity correction surgery, is characterized by rapid neuronal loss. However, the molecular mechanisms linking mechanical distraction to apoptosis remain unclear. Here, we tested whether sodium rutin (NaR), a water-soluble rutin derivative with improved oral bioavailability, mitigates DSCI. **Methods:** We employed an *in vivo* rat DSCI model and an *in vitro* mechanical distraction (DIS) model using neuronal cells. The therapeutic efficacy of NaR was evaluated using locomotor function assessments (Basso–Beattie–Bresnahan score and footprint analysis), histopathology, and transmission electron microscopy. Molecular docking simulations were performed to predict the binding affinity of NaR to Erb-B2 receptor tyrosine kinase 4 (ErbB4). Mechanistic investigations targeting the ErbB4/protein kinase B (Akt) axis, reactive oxygen species (ROS), and apoptotic pathways were conducted using western blot analysis and immunofluorescence. **Results:** DIS suppressed ErbB4 phosphorylation and downstream Akt signaling, accompanied by the activation of B-cell lymphoma 2/Bcl-2-associated X protein/Caspase-3 (Bcl-2/Bax/Caspase-3) apoptotic pathways after DSCI. Simultaneously, DIS induced a decrease in the mitochondrial membrane potential ($\Delta\Psi m$) and accumulation of mitochondrial ROS, along with a significant reduction in superoxide dismutase 2 (SOD2) and glutathione peroxidase 4 (GPX4) levels. NaR treatment engaged ErbB4 to restore ErbB4/Akt signaling, inhibited mitochondrial ROS signaling, ameliorated $\Delta\Psi m$, and reduced the number of terminal deoxynucleotidyl transferase dUTP nick end labeling (TUNEL)-positive apoptotic neurons, thereby inhibiting neuronal apoptosis. However, the inhibition of ErbB4 phosphorylation along with NaR treatment significantly reversed these therapeutic effects. Furthermore, the pharmacological administration of NaR ameliorated histopathological and neuronal ultrastructural damage in the spinal cord tissues, increased the number of surviving neurons, and facilitated locomotor recovery after DSCI. **Conclusions:** These findings identify ErbB4 and ROS signaling as key regulators of neuronal survival during DSCI and establish NaR as a candidate therapeutic strategy for DSCI associated with spinal deformity correction surgery.

Keywords: spinal cord injuries; sodium rutin; ErbB4/Akt signaling; neuronal apoptosis; oxidative stress

1. Introduction

Distractive spinal cord injury (DSCI) is a severe complication of spinal deformity correction surgery for conditions such as scoliosis and kyphosis and occurs with increased frequency in patients with severe deformities [1]. The reported incidence of DSCI during correction procedures ranges from 2.6% to 7%, making it a major cause of postoperative neurological dysfunction [2]. Unlike high-energy traumatic injuries, such as spinal cord contusion or transection, DSCI arises from sustained tensile forces applied to the spinal cord. Progressive neuronal loss is a central pathological feature underlying the permanent neurological deficits associated with DSCI [3]. Although the primary mechanical insult initiates tissue damage in spinal cord injuries (SCIs), accumulating evidence indicates that neuronal death predominantly results from secondary injury cascades, including oxidative stress, protein misfolding, and inflammation [4,5,6]. However, the molecular mechanisms linking sustained mechanical distraction (DIS) to neuronal apoptosis remain incompletely defined, and effective targeted pharmacological interventions are limited.

Rutin, a natural flavonoid, has attracted considerable attention for its antioxidant, anti-apoptotic, and anti-inflammatory properties [7]. Although rutin shows neuroprotective potential in central nervous system (CNS) injury, its poor aqueous solubility and limited bioavailability have

hindered mechanistic investigations and clinical translation [8]. In our previous studies [9,10], we generated a sodium salt derivative of rutin (sodium rutin, NaR) with substantially improved water solubility, oral bioavailability, and blood-brain barrier permeability [10]. Enhanced penetration enabled drug accumulation at spinal lesion sites, providing a pharmacokinetic basis for evaluating NaR as a therapeutic candidate for DSCI. Whether NaR can mitigate neuronal apoptosis induced by sustained DIS, and through which molecular pathways it acts, however, remains unknown.

Erb-B2 receptor tyrosine kinase 4 (ErbB4) is widely expressed in the CNS and regulates neuronal survival, migration, and neurite outgrowth among others [11]. Upon binding to its ligand, neuregulin-1, ErbB4 forms heterodimers with ErbB2 and activates the downstream phosphoinositide 3-kinase (PI3K)–protein kinase B (Akt) signaling pathway that promotes neuronal survival, repair, and metabolic homeostasis after CNS injury [12,13]. Dysregulation of ErbB4 has been implicated in multiple neurological disorders, including ischemic stroke, SCI, and neurodegenerative diseases [4,14]. Although ErbB4 is recognized for its neuroprotective effect in brain injuries, its specific function in SCI remains incompletely understood. Notably, systematic bioinformatic analyses of SCI datasets have identified ErbB4 as a potential therapeutic target with mechanosensitive properties relevant to DSCI [15]. Experimental studies have further indicated that phosphorylated ErbB4 (p-ErbB4) levels are reduced after SCI and that restoration of ErbB4 signaling promotes neuronal survival through PI3K/Akt activation [4,16]. Despite these findings, whether suppression of ErbB4 signaling contributes to neuronal apoptosis under sustained DIS stress, and how this pathway intersects with mitochondrial injury, remain unclear.

Mitochondrial oxidative stress is a key driver of neuronal apoptosis, with mitochondria serving as central regulators of reactive oxygen species (ROS) homeostasis [17,18]. Within the mitochondrial matrix, superoxide dismutase 2 (SOD2) converts superoxide anions to hydrogen peroxide, which is detoxified by glutathione peroxidase 4 (GPX4), forming a coordinated antioxidant defense system [19]. Previous evidence also suggested that ErbB4 signaling can suppress ROS-mediated apoptosis through PI3K/Akt activation [20]. However, the changes in mitochondrial ROS levels after DSCI and their role in neuronal apoptosis following DSCI have not been defined.

Here, we investigated whether DIS regulates ErbB4 and ROS signaling to trigger neuronal apoptosis and whether NaR can attenuate these effects. We showed that mechanical DIS reduces ErbB4/Akt pathway activation, activates ROS signaling, and induces mitochondrial dysfunction and activation of intrinsic apoptotic pathways. Pharmacological administration of NaR restores ErbB4 and ROS signaling, enhances mitochondrial antioxidant capacity, alleviates neuronal apoptosis, and improves functional recovery after DSCI. These findings indicate that ErbB4 and ROS signaling link mechanical DIS to neuronal apoptosis and support NaR as a potential therapeutic strategy for DSCI.

2. Materials and Methods

2.1 Reagents

NaR was synthesized by our group according to previously reported protocols and patents (CN201810227319.6 and CN201821671201.4) [9,10]. Dacomitinib (Dac), an ErbB4 inhibitor, was obtained from MedChemExpress (MCE, Monmouth Junction, NJ, USA; Cat# HY-13272).

2.2 Neuronal Cell Lines and Culture

VSC4.1 motor neuron–like cells were obtained from Fenghui Biotechnology (Changsha, Hunan, China; Cat# CL0674). SH-SY5Y cells (RRID: CVCL_0019) were obtained from the Cell Bank of the Chinese Academy of Sciences (Shanghai, China). All cell lines were authenticated via short tandem repeat profiling and routinely tested negative for mycoplasma by polymerase chain reaction. Cells were cultured in DMEM (Gibco, Grand Island, NY, USA; Cat# 11995065) supplemented with 10% fetal bovine serum (FBS, Gibco, USA; Cat# 10099141C) at 37 °C in 5% CO_2.

2.3 Establishment of the in vitro Mechanical Distraction Model

The neuronal cells were seeded onto BioFlex® type I collagen–coated six-well plates (Flexcell International Corporation, Burlington, NC, USA; Cat# BF-3001C) and allowed to adhere overnight. When the cultures reached approximately 80% confluence, mechanical DIS was applied using a Flexcell-5000T™ Tension System (Flexcell International Corporation, Burlington, NC, USA). A constant 10% static DIS was applied to neuronal cells for 6 h to simulate the sustained DIS stress experienced by neurons during the acute phase of clinical DSCI [21]. Meanwhile, the control group was maintained in the same environment but was spared from any mechanical DIS.

2.4 Establishment of the DSCI Rat Model

Prior to surgery, the rats were anesthetized via an intraperitoneal injection of sodium pentobarbital (50 mg/kg) to ensure a deep surgical plane and abolish pain reflexes. The DSCI rat model was generated as previously described [8]. A custom spinal distraction device (Patent No. CN202220982496.7) was used to distract the T11–T12 intervertebral space by 1 cm for 15 min. Rigid internal fixation was then performed using a custom fixator (Patent No. CN202420096029.3). Successful model induction was confirmed by a postoperative Basso–Beattie–Bresnahan (BBB) score of 0. At the designated experimental endpoints, all animals were humanely euthanized via an intraperitoneal injection of an overdose of sodium pentobarbital (200 mg/kg).

2.5 Grouping and Drug Administration

Drug administration for the four rat groups began on postoperative day 1 and continued for 28 days. NaR was dissolved in sterile 0.9% NaCl. The rats that underwent DSCI surgery were randomly allocated into three groups: a DSCI model group and two NaR treatment groups, which received NaR via oral gavage at a low dose NaR (LNaR, 25 mg/kg/day) or a high dose NaR (HNaR, 50 mg/kg/day) [9]. Rats in the Sham and the DSCI group received an equivalent volume of 0.9% NaCl. Rats were maintained in a standard laboratory environment under a 12-h light/dark cycle and provided with *ad libitum* access to food and water.

Based on the clinical dosage of troxerutin and previously validated *in vitro* NaR intervention protocols [10], the neuronal cells were pre-treated with NaR (20 μg/mL) or vehicle (PBS) and cultured for 24 h. Prior to a 6-hour mechanical DIS, cells were pre-treated with 73.7 nM Dacomitinib (Dac) for 2 h [22]. Neuronal cells were divided into four groups. The normal control (NC) group received PBS without mechanical DIS. The remaining three groups were subjected to a 6-hour mechanical DIS following their respective pretreatments: the DIS group (PBS for 24 h), the NaR group (20 μg/mL NaR for 24 h), and the NaR + Dac group (20 μg/mL NaR for 24 h and 73.7 nM dacomitinib for 2 h).

2.6 Behavioral Assessment

Locomotor function changes were assessed using the BBB scale at 1–28 days post-injury (dpi) [23]. Footprint analysis was performed at 28 dpi, as described previously [8]. The animals were prompted to traverse a straight corridor following the application of red and blue dyes to their forelimbs and hindlimbs, respectively. Stride length was quantified from footprint images.

2.7 Molecular Docking Simulation

Because the full-length crystal structure of ErbB4 is not available, a three-dimensional model (UniProt Q15303) was generated using AlphaFold3 (Google DeepMind, London, UK). The chemical structure of NaR was constructed with deprotonation of the 7-hydroxyl group of rutin to form the sodium salt. The ligand structure was sketched in ChemOffice 14.0 (Revvity Signals Software, Waltham, MA, USA), and the energy was minimized using Chem3D.

Potential binding pockets were identified using AutoLigand 1.5.6 (The Scripps Research Institute, La Jolla, CA, USA) with a blind docking approach. Molecular docking was performed using AutoDock Vina 1.2.5 (The Scripps Research Institute). The AutoDockTools 1.5.6 software package (The Scripps Research Institute) was employed for the structural preparation of both receptors and ligands. NaR was docked into 10 predicted binding sites and ranked by binding energy, estimated inhibition constant (Ki), and ligand efficiency. The highest-affinity pose was analyzed using PyMOL 3.1 (Schrödinger, New York, NY, USA) and Discovery Studio 2024 (BIOVIA, San Diego, CA, USA).

2.8 Histological Analysis

Animals were euthanized at 3 dpi and 28 dpi. Spinal cord tissues were routinely fixed, embedded in paraffin, and sectioned at 4 μm. Sections were stained using a hematoxylin and eosin (H&E) kit (Servicebio, Wuhan, Hubei, China; Cat# G1076), and a Nissl staining Kit (Servicebio, Cat# G1086). Slides were scanned using a NanoZoomer S60 digital slide scanner (Hamamatsu Photonics, Hamamatsu, Japan). Histological scoring [24] and the number of Nissl-positive neurons were quantified as described previously [25].

2.9 Transmission Electron Microscopy (TEM)

Ultrathin sections (90 nm) were stained with uranyl acetate and lead citrate and imaged using a JEM-100SX transmission electron microscope (JEOL, Tokyo, Japan). The pathological changes of neuronal and myelin ultrastructure were analyzed.

2.10 Immunofluorescence (IF)

Conventional IF staining was conducted on cultured neuronal cells and spinal cord sections as described previously [8]. Images were captured using a confocal fluorescence microscope (TCS SP8 STED, Leica Microsystems, Wetzlar, Germany). For quantitative analysis, multiple non-serial tissue sections per animal were analyzed using ImageJ 1.53t (NIH, Bethesda, MD, USA). Antibody details are provided in **Supplementary Table 1**.

2.11 Terminal Deoxynucleotidyl Transferase dUTP Nick end Labeling (TUNEL) Staining

Neuronal apoptosis was evaluated with a TUNEL staining Kit (Servicebio, Wuhan, Hubei, China; Cat# G1504-50T) combined with NeuN immunofluorescence. After permeabilization and blocking, the sections were treated with an anti-NeuN (Abcam, Waltham, MA, USA; Cat# ab104224) antibody followed by a secondary antibody. The slides were equilibrated and incubated with the TUNEL reaction mixture, followed by nuclear counterstaining with 4',6-diamidino-2-phenylindole (DAPI, Beyotime, Shanghai, China; Cat# C1002). Images were acquired using a Leica confocal fluorescence microscope. Positive cells were quantified from identical anatomical regions in eight rats per group using ImageJ [26].

2.12 Western Blot

Cells were lysed and protein concentrations were determined. Subsequently, Western blot assays were routinely performed as previously described [8]. Signals were detected using enhanced chemiluminescence reagents and imaged using a FluorChem FC3 system (ProteinSimple, San Jose, CA, USA). Band intensity was quantified using ImageJ. The antibody information is listed in **Supplementary Table 1**.

2.13 Measurement of Intracellular ROS, Mitochondrial ROS and ΔΨm

The three indicators were detected using kits for 2′,7′-dichlorodihydrofluorescein diacetate (DCFH-DA, Beyotime, Cat# S1105S) [27], MitoSOX Red mitochondrial superoxide indicator (MitoSOX, Beyotime, Cat# S0061S) [5] and 5,5′,6,6′-tetrachloro-1,1′,3,3′-tetraethylbenzimidazolylcarbocyanine iodide (JC-1, Beyotime, Cat# C1475S). The ΔΨm was calculated as the ratio of red (JC-1 aggregates) to green (monomers) fluorescence. Live-cell mitochondria were labeled with MitoTracker Green (Beyotime, Cat# C1048), and nuclei were counterstained with Hoechst 33342 (Servicebio, Cat# G1127). Fluorescence images were captured using a confocal fluorescence microscope and analyzed using ImageJ.

2.14 Statistical Analyses

All quantitative experiments were performed with at least three independent biological replicates. Randomization and blinding were employed for all behavioral assessments and histological quantification, with analyses conducted by two investigators blinded to the experimental condition. Data are presented as mean ± standard deviation (SD). Statistical analyses were conducted using GraphPad Prism 10 (GraphPad Software, San Diego, CA, USA). Two-group comparisons were performed using two-tailed Student's *t* tests. Multiple comparisons were analyzed with one-way analysis of variance followed by Tukey's post hoc test. Statistical significance was set at $p < 0.05$.

3. Results

3.1 NaR Attenuates Neuronal Apoptosis and Promotes Locomotor Recovery After DSCI

To evaluate the therapeutic effects of NaR on functional recovery after DSCI, locomotor behavior was assessed at 1, 3, 7, 14, 21, and 28 dpi (Fig. 1A). Rats subjected to DSCI exhibited severe locomotor impairment, with BBB scores remaining significantly lower than those of all other groups from 7 to 28 dpi (Fig. 1B). Treatment with low- or high-dose NaR significantly improved locomotor recovery beginning at 7 dpi, with sustained improvement through 28 dpi. Recovery was more pronounced in the HNaR group ($p < 0.05$). These functional improvements were corroborated by footprint analysis at 28 dpi (Fig. 1C). Rats in the DSCI group displayed marked hindlimb dragging and impaired coordination, whereas NaR-treated animals showed improved stepping patterns. HNaR treatment produced more coordinated hindlimb movement and significantly increased stride length in a dose-dependent manner compared with the untreated DSCI group (Fig. 1C).

Histopathological analysis at 3 dpi revealed pronounced structural disruption of the white and gray matter after DSCI, accompanied by hemorrhage, axonal edema, and neuronal loss (Fig. 1D). Histopathological scores were significantly elevated in the DSCI group compared to those in the sham group ($p < 0.001$). NaR treatment reduced tissue disruption and neuronal loss, resulting in significantly lower histopathological scores (Fig. 1D). Because apoptosis is a major contributor to neuronal loss during the early post-injury phase [28,29], we performed TUNEL staining at 3 dpi. The proportion of TUNEL-positive neurons markedly increased after DSCI but was significantly reduced by NaR treatment in a dose-dependent manner (Fig. 1E). Together, these results indicate that NaR improves functional recovery and attenuates neuronal apoptosis after DSCI.

3.2 NaR Ameliorates Neuronal Ultrastructural Damage in Spinal Cord Tissue After DSCI

We performed TEM at 3 dpi to determine whether NaR preserves spinal cord neuronal and myelin ultrastructure after DSCI. Neurons in the sham group exhibited preserved ultrastructural integrity, including distinct nucleoli and abundant mitochondria with well-defined cristae (Fig. 2A). In contrast, neurons in the DSCI group displayed marked ultrastructural disruption, characterized by nuclear shrinkage, irregular nuclear membranes, and extensive cytoplasmic organelle damage. Mitochondria appeared swollen and vacuolated with disrupted cristae, and the endoplasmic reticulum was dilated. NaR treatment attenuated these ultrastructural abnormalities; the HNaR group showed the most pronounced protection, with neuronal organelles resembling those observed in sham controls.

TEM morphological analyses further characterized the changes in myelin and axonal structure after DSCI (Fig. 2B). The sham group showed compact myelinated axons. In the untreated DSCI group, axons were swollen and separated, and myelin sheaths were loose, disorganized, and ruptured, consistent with intramyelinic edema. NaR treatment improved these ultrastructural abnormalities, and alleviated demyelination and intramyelinic edema. Together, these findings indicate that NaR preserves neuronal and axonal ultrastructure and mitigates myelin pathology after DSCI.

3.3 NaR Promotes ErbB4 Phosphorylation and Activates ErbB4/Akt Signaling After DSCI

Previous large-scale sequencing analyses identified ErbB4 as a potential therapeutic target in SCI [15]. Phosphorylation of ErbB4 has been linked to improved functional recovery after SCI [4,16]. We performed molecular docking analysis to investigate the potential binding affinity between NaR and ErbB4 (Fig. 3A,B). Ten potential binding pockets were identified and ranked according to their docking scores, with NaR showing the highest affinity for the top-ranked pocket. The predicted binding energy was −9.5 kcal/mol, and NaR fit within the active pocket through multiple hydrophilic and hydrophobic interactions.

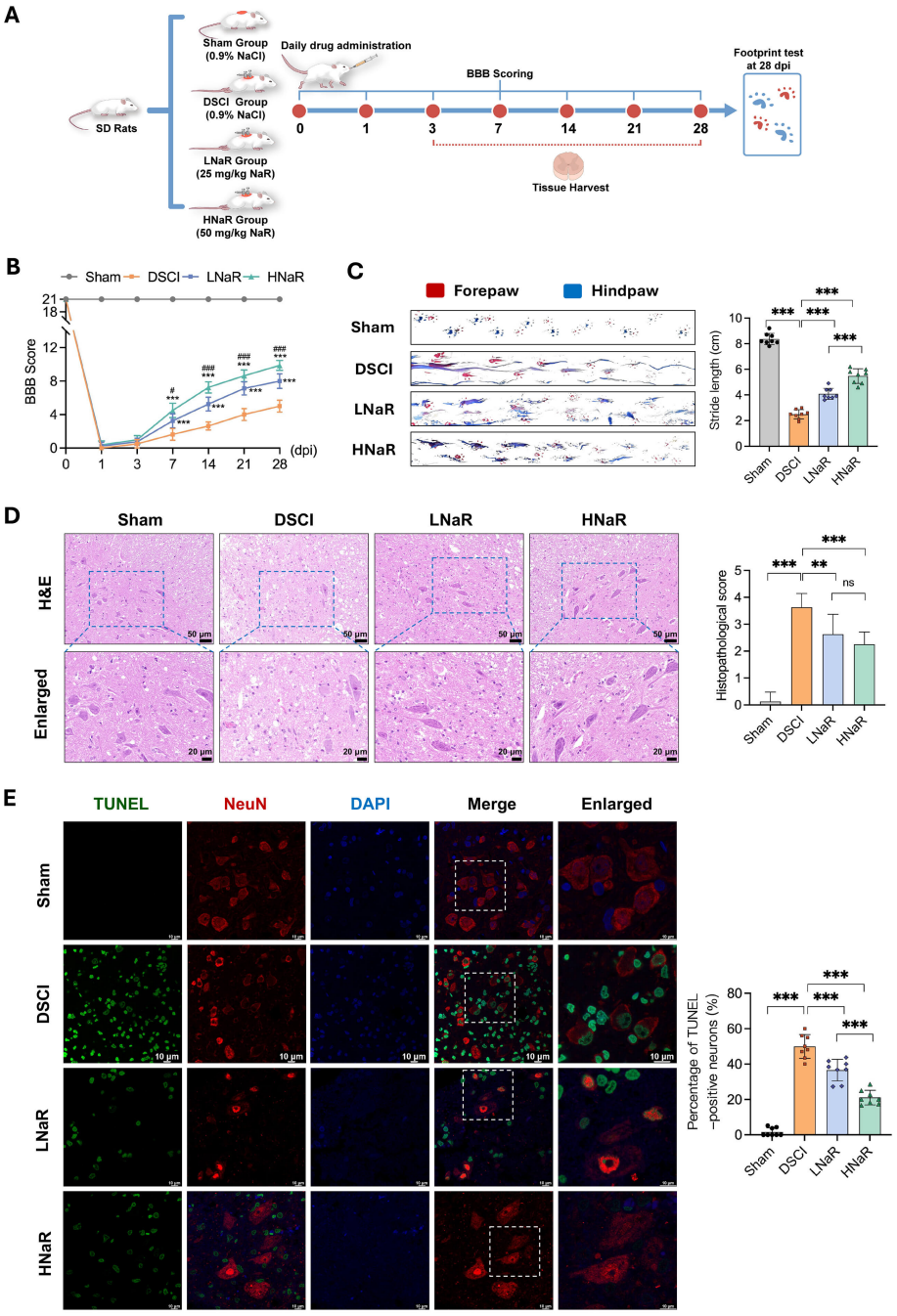

Fig. 1. NaR attenuates neuronal apoptosis and promotes locomotor recovery after DSCI. (A) Experimental design and timeline. Rats were assigned to sham, DSCI, or NaR treatment groups. Behavioral testing, drug administration, and tissue collection were performed at the indicated time points. (B) Hindlimb locomotor function was assessed by BBB scoring from 1 to 28 dpi (n = 8). (C) Representative footprint patterns at 28 dpi. Forepaws were labeled with red ink and hindpaws with blue ink. Quantification of stride length is shown (n = 8). (D) H&E staining of spinal cord tissue at 3 dpi. Histopathological scores were quantified to assess the severity of tissue damage (n = 8). Scale bar = 50 or 20 μm. (E) TUNEL staining at 3 dpi. TUNEL-positive apoptotic cells are shown in green, and neurons are labeled with NeuN (red). The dashed box for the representative region of the merged channel was enlarged. Quantification of TUNEL-positive neurons is shown (n = 8). Scale bar = 10 μm. Data are presented as mean ± SD. $^{\#}p < 0.05$, $^{\#\#\#}p < 0.001$ vs. LNaR group; $^{**}p < 0.01$, $^{***}p < 0.001$ vs. DSCI group; ns: not significant. NaR, sodium rutin; DSCI, distractive spinal cord injury; BBB, Basso–Beattie–Bresnahan; dpi, days post injury; H&E, hematoxylin and eosin; TUNEL, terminal deoxynucleotidyl transferase dUTP nick end labeling; SD, standard deviation; LNaR, low dose NaR; HNaR, high dose NaR; DAPI, 4',6-diamidino-2-phenylindole.

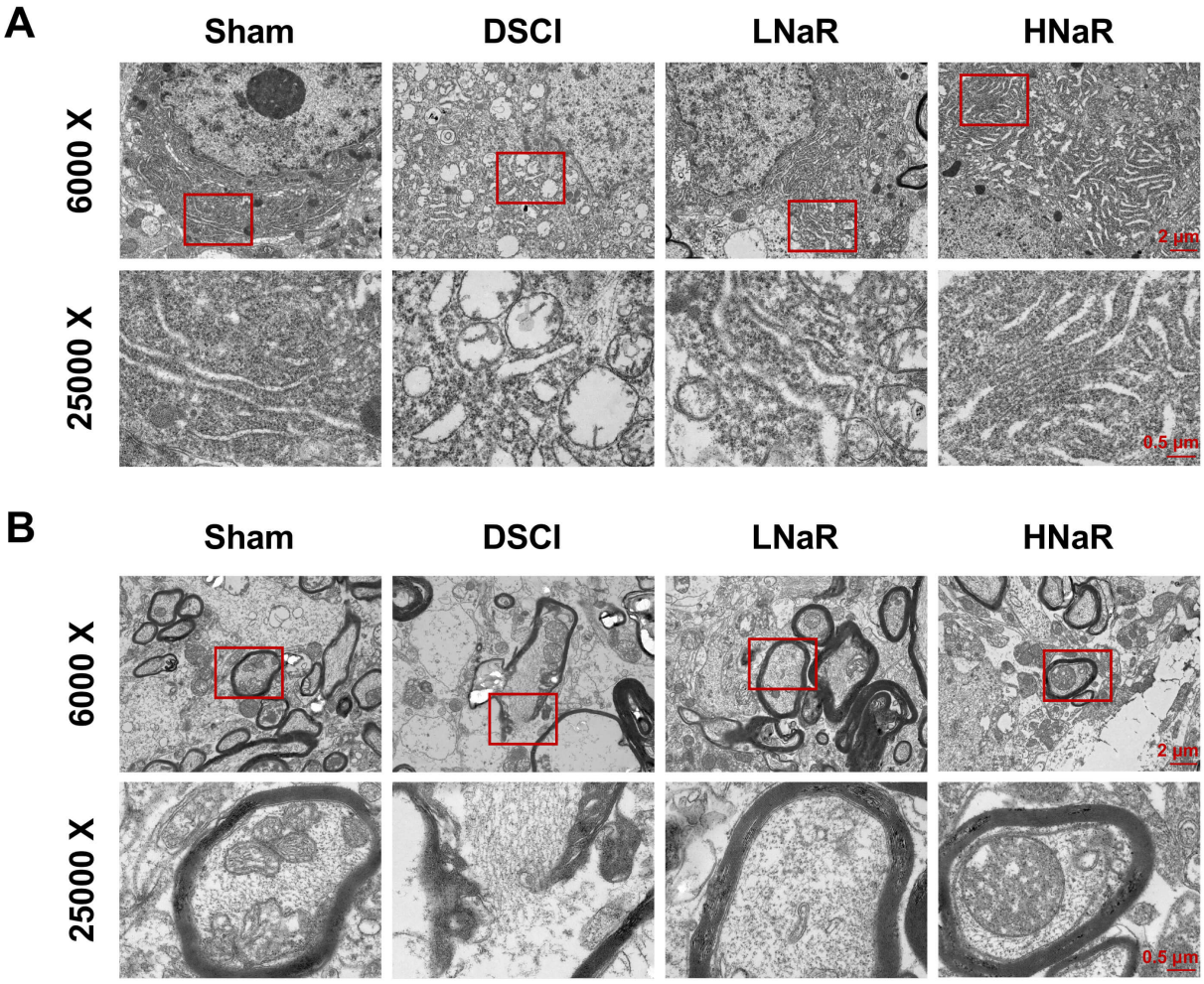

Fig. 2. NaR ameliorates neuronal and myelin ultrastructural damage in spinal cord tissues after DSCI. (A) Representative TEM images of neuronal cell bodies in spinal cord tissue at 3 dpi. Top row, low magnification (6000×); the regions within the red boxes were further magnified at a higher magnification (bottom row, 25,000×). Scale bars: 2 μm (top) and 0.5 μm (bottom). (B) Representative TEM images of myelinated axons. The regions within the red boxes in the top row (top, 6000×) are further shown at a higher magnification (bottom, 25,000×). Scale bars: 2 μm (top) and 0.5 μm (bottom). TEM, transmission electron microscopy.

We assessed ErbB4 phosphorylation in spinal cord tissue to validate these findings *in vivo* (Fig. 3C). IF staining showed that p-ErbB4 levels in NeuN-positive ($NeuN^+$) neurons were significantly reduced after DSCI. NaR treatment restored neuronal p-ErbB4 expression in a dose-dependent manner. Because ErbB4/Akt signaling supports neuronal survival and repair after SCI [4,16], we next examined this pathway *in vitro* using VSC4.1 motor neurons subjected to DIS (Fig. 3D, the original Western blot images are available in the **Supplementary Material-WB images**). Western blot analysis demonstrated that DIS suppressed the phosphorylation of both ErbB4 and Akt, whereas NaR treatment restored the phosphorylation of these proteins. Notably, the NaR-induced activation of ErbB4/Akt was reversed by the ErbB4 inhibitor Dac. Together, these data indicate that NaR activates the ErbB4/Akt signaling pathway in a manner that depends on its promotion of ErbB4 phosphorylation after DSCI.

3.4 NaR Inhibits Neuronal Apoptosis Through the B-cell Lymphoma 2 (Bcl-2)/Bcl-2-associated X Protein (Bax)/Caspase-3 Pathway by Activating ErbB4/Akt Signaling After DSCI

To determine whether NaR suppresses apoptosis through this pathway, we examined apoptotic markers in SH-SY5Y cells subjected to DIS (Fig. 4A, the original Western blot images are available in the **Supplementary Material-WB images**). Western blot analysis showed that DIS reduced the anti-apoptotic protein Bcl-2 and increased the pro-apoptotic proteins Bax and cleaved Caspase-3. NaR treatment reversed these changes, restoring Bcl-2 levels while reducing Bax and cleaved Caspase-3 expression. Notably, the upregulation of Bcl-2 and downregulation of Bax and Caspase-3 expression by NaR could be reversed by the ErbB4 inhibitor Dac. IF analysis in DIS cells confirmed these findings and revealed significantly reduced intracellular cleaved Caspase-3 after NaR treatment, which could be

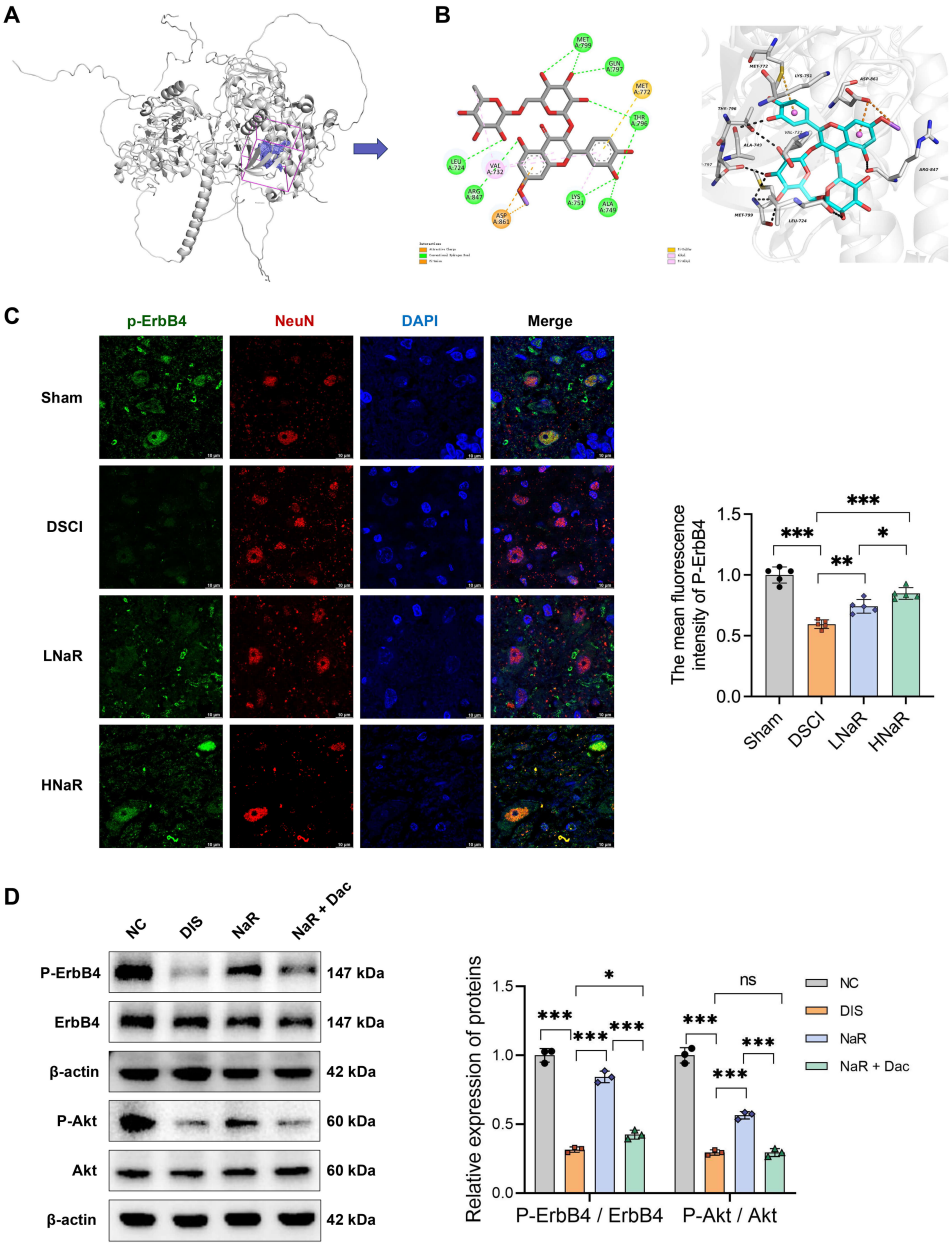

Fig. 3. NaR promotes ErbB4 phosphorylation and activates ErbB4/Akt signaling after DSCI. (A) Identification of potential NaR-binding pockets in ErbB4 using molecular docking. Ten candidate pockets were ranked by docking score, and the highest-affinity pocket was highlighted. (B) Predicted interaction between NaR and ErbB4. Left panel: 2D interaction diagram showing the key residues involved in hydrogen bonding (green dotted line), "π-sulfur" (yellow dotted line, Met772), electrostatic interactions (orange dotted line, Asp861), and hydrophobic interactions (pink dotted line, VAL732). Right panel: 3D structural representation of the NaR–ErbB4 complex binding pocket. The ErbB4 protein backbone is shown as white ribbons, and the NaR ligand is displayed as cyan sticks. Key interacting residues are labeled and shown as grey sticks. Black dashed lines represent the hydrogen bond network stabilizing the complex. (C) Immunofluorescence analysis of p-ErbB4 in $NeuN^+$ neurons in spinal cord tissue. p-ErbB4 is shown in green, NeuN in red, and nuclei are counterstained with DAPI (blue). Quantification of the fluorescence intensity is presented (n = 5). Scale bar = 10 μm. (D) Western blot analysis of p-ErbB4/ErbB4 and p-Akt/Akt in VSC4.1 cells from normal control (NC), DIS, NaR, and NaR + Dacomitinib (Dac) groups (n = 3). Data are presented as mean ± SD. *$p < 0.05$, **$p < 0.01$, ***$p < 0.001$ for comparisons between groups. ns: not significant; ErbB4, Erb-B2 receptor tyrosine kinase 4; Akt, protein kinase B; p-ErbB4, phosphorylated ErbB4; $NeuN^+$, NeuN-positive; DIS, distraction; Dac, Dacomitinib.

reversed by Dac (Fig. 4B). We assessed cleaved Caspase-3 expression in spinal cord neurons at 3 dpi to validate these observations *in vivo*. Cleaved Caspase-3 levels were markedly elevated in neurons after DSCI but were significantly reduced by NaR treatment in a dose-dependent manner (Fig. 4C). Together, these results indicate that NaR suppresses the intrinsic apoptotic program involving Bcl-2, Bax, and Caspase-3 by activating ErbB4/Akt signaling, thereby preserving neuronal viability after DSCI.

3.5 NaR Alleviates Mitochondrial Oxidative Stress and Dysfunction

To further define how NaR preserves neuronal integrity, we examined mitochondrial oxidative stress, a key upstream driver of neuronal apoptosis [30]. Total intracellular ROS and mitochondrial ROS (mtROS) were detected using DCFH-DA (Fig. 5A) and MitoSOX staining (Fig. 5B), respectively. DIS markedly increased both total intracellular ROS and mtROS levels, whereas NaR treatment significantly attenuated this accumulation. Loss of mitochondrial membrane potential (MMP; $\Delta\Psi m$) is a hallmark of mitochondrial apoptotic initiation [31]. We therefore assessed MMP changes using JC-1 staining (Fig. 5C). DIS induced pronounced mitochondrial depolarization, while NaR treatment restored MMP toward control levels. Together, these data indicate that NaR suppresses mechanical DIS-induced mitochondrial oxidative stress, preserves mitochondrial function, and limits the activation of the mitochondria-dependent apoptotic pathway.

3.6 NaR Attenuates Mitochondrial Oxidative Stress by Upregulating SOD2 and GPX4

To determine whether NaR modulates mitochondrial antioxidant defenses after DSCI, protein expression was assessed in SH-SY5Y cells subjected to DIS using western blot analysis. We found that DIS reduced SOD2 and GPX4 protein levels, whereas NaR treatment restored their expression (Fig. 6A, the original Western blot images are available in the **Supplementary Material-WB images**). Consistent with the *in vitro* findings, we next examined the expression of SOD2 and GPX4 in spinal cord neurons at 3 dpi (Fig. 6B,C). IF analysis showed that SOD2 and GPX4 expression in $NeuN^+$ neurons was markedly reduced after DSCI compared to that in sham controls. NaR treatment restored the expression of both antioxidant enzymes in a dose-dependent manner. Together, these results indicate that NaR enhances mitochondrial antioxidant capacity by upregulating SOD2 and GPX4, which is consistent with the reduced oxidative stress and suppression of mitochondria-dependent apoptotic signaling after DSCI.

3.7 NaR Significantly Promotes Motor Neuron Survival Following DSCI

Nissl staining demonstrated a significant reduction in the number of surviving motor neurons in the anterior horn of the spinal cord at 28 days post-DSCI compared to the sham group ($p < 0.001$) (Fig. 7). However, treatment with either dose of NaR effectively rescued this neuronal loss, and the HNaR group exhibited superior neuroprotective efficacy ($p < 0.001$). These findings indicate that pharmacological administration of NaR after injury exerts a profound and sustained protective effect on anterior horn motor neurons after DSCI.

4. Discussion

DSCI represents a distinct and clinically challenging form of SCIs that fundamentally differs from high-energy contusion or transection injuries [6,32,33]. Based on our clinical experience in managing SCI, therapeutic strategies developed for transient high-energy trauma are unsuitable for the low-energy, sustained DIS forces that characterize DSCI, largely because of the lack of defined mechanosensitive therapeutic targets [1,34,35]. Therefore, effective treatment of DSCI requires the identification of molecular pathways that specifically respond to mechanical DIS [1]. Current approaches remain limited in part because the mechanobiological processes that convert sustained mechanical DIS stress into neuronal injury are poorly understood. In this study, we established *in vivo* and *in vitro* models of neuronal injury induced by mechanical DIS and identified a mechanotransduction cascade linking DIS stress to neuronal apoptosis. Mechanical DIS suppressed ErbB4/Akt signaling, increased mitochondrial ROS production, and activated the Bcl-2/Bax/Caspase-3 apoptotic pathway. Systemic administration of NaR, together with *in vitro* intervention, restored ErbB4/Akt signaling, reduced mitochondrial ROS, suppressed neuronal apoptosis, and improved locomotor recovery after DSCI. These findings identify a mechanosensitive signaling axis through which mechanical DIS drives neuronal injury and demonstrate that pharmacological activation of this pathway confers neuroprotection (Fig. 8).

ErbB4 is a neuroprotective receptor with established roles in cell survival and oxidative stress regulation and exhibits features consistent with mechanosensitive signaling [36,37]. Previous studies have documented ErbB4 expression in brain injury models, and its role in SCI has received increasing attention [4,16]. Upon activation, ErbB4 undergoes proteolytic cleavage to generate an intracellular domain capable of regulating transcriptional programs linked to neuronal survival and glial responses [38]. Our data indicate that neurons subjected to sustained mechanical DIS exhibit reduced ErbB4 expression and phosphorylation, suggesting that disruption of this pathway is an early event in DIS-induced injury. Docking analyses supported a high predicted binding affinity between NaR and ErbB4, providing a structural basis for the putative NaR–ErbB4 interaction that may underlie the observed increase in ErbB4 phosphorylation. Consistent with this interpretation, NaR restored ErbB4 phosphorylation and downstream Akt sig-

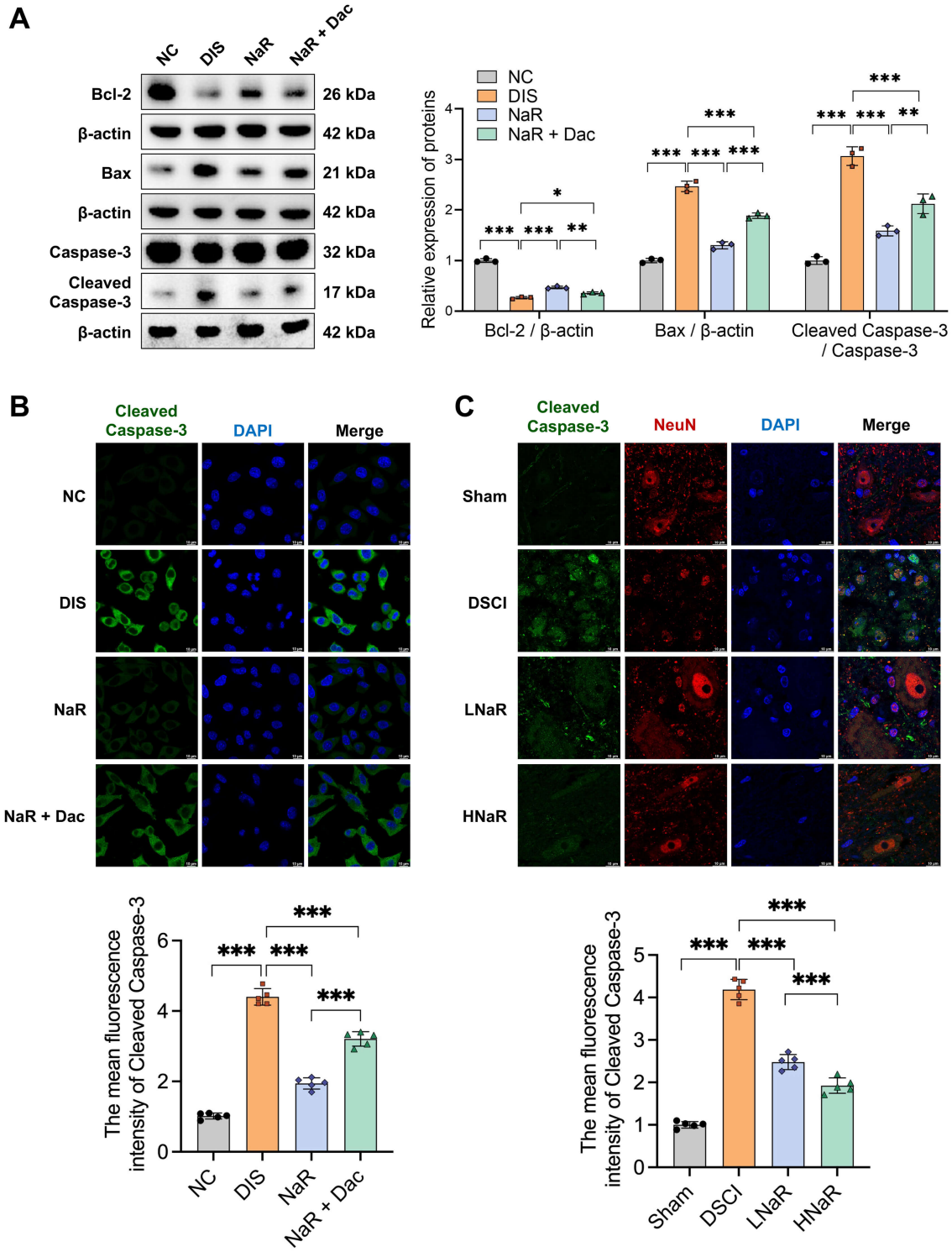

Fig. 4. NaR inhibits neuronal apoptosis through the ErbB4/Akt–Bcl-2/Bax/Caspase-3 pathway after DSCI. (A) Representative western blots and quantification of Bcl-2, Bax, and cleaved Caspase-3 in SH-SY5Y cells subjected to DIS, NaR and NaR + Dac (n = 3). (B) Immunofluorescence analysis of cleaved Caspase-3 in VSC4.1 cells from control (NC), DIS, NaR and NaR + Dac groups (n = 5). Cleaved Caspase-3 is shown in green, and nuclei are counterstained with DAPI (blue). Scale bar = 10 μm. (C) Immunofluorescence analysis of cleaved-Caspase-3 in spinal cord ($NeuN^+$) neurons from the sham, DSCI, and NaR groups. Cleaved-Caspase-3 is shown in green, NeuN in red, and nuclei are counterstained with DAPI (blue). Scale bar = 10 μm. Quantification of fluorescence intensity is shown (n = 5). Data are presented as mean ± SD. *$p < 0.05$, **$p < 0.01$, ***$p < 0.001$ for comparisons between groups.

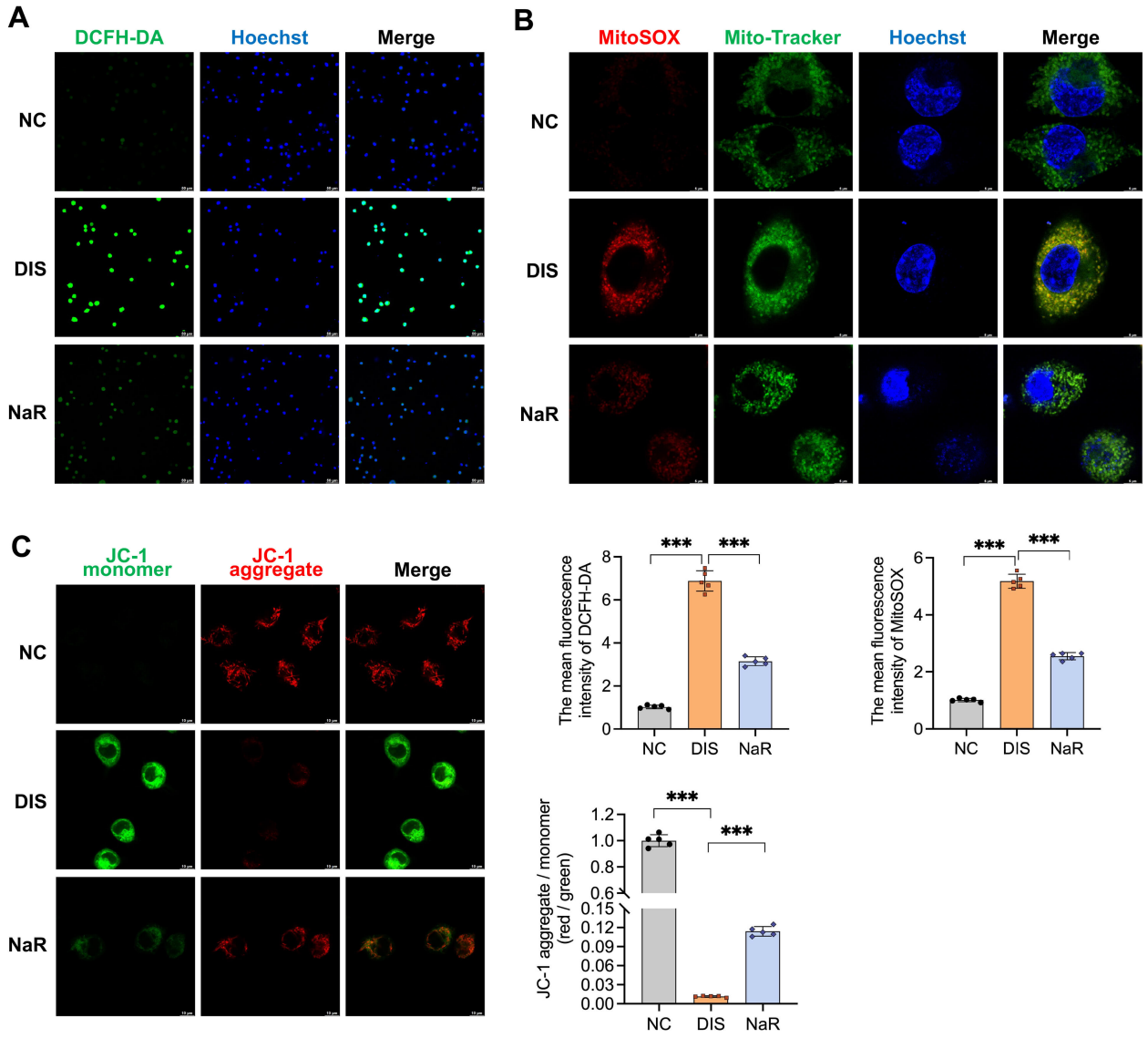

Fig. 5. NaR alleviates mitochondrial dysfunction and oxidative stress. (A) Measurement of intracellular ROS levels in VSC4.1 cells (n = 5). Representative fluorescence images show cells stained with DCFH-DA (green) and nuclei counterstained with Hoechst 33342 (blue) in the NC, DIS, and NaR-treated groups. Scale bar = 50 μm. (B) Assessment of mitochondrial ROS levels (n = 5). Representative confocal images of VSC4.1 cells stained with MitoSOX Red (red) and MitoTracker Green (green) and nuclei counterstained with Hoechst 33342 (blue). Scale bar = 5 μm. (C) Evaluation of mitochondrial membrane potential (ΔΨm) using JC-1 staining (n = 5). Representative fluorescence images show JC-1 aggregates (red, high ΔΨm) and monomers (green, low ΔΨm). Scale bar =10 μm. Data are presented as mean ± SD. ***$p < 0.001$ for comparisons between groups. DCFH-DA, 2′,7′-dichlorodihydrofluorescein diacetate; ROS, reactive oxygen species; JC-1, 5,5′,6,6′-tetrachloro-1,1′,3,3′-tetraethylbenzimidazolylcarbocyanine iodide.

naling both *in vivo* and *in vitro*; notably, these effects were effectively abrogated by the ErbB4 inhibitor Dac. Activation of this survival pathway likely contributes to resistance against DIS-induced apoptosis and aligns with previous reports implicating ErbB4/Akt signaling in neuroprotection in SCI and in other neurological disorders [20,39].

The association between the restoration of ErbB4 signaling and improved locomotor recovery suggests that ErbB4 functions as a mechanosensitive signaling node in DSCI. Studies in other systems have linked ErbB4 to synaptic plasticity and to mechanosensitive pathways, such as Hippo–Yes-associated protein (YAP)/transcriptional coactivator with PDZ-binding motif (TAZ) signaling [40], and the neuregulin 1–ErbB4 axis has been shown to respond to cytoskeleton tension during cardiomyocyte maturation and proliferation [36]. In the spinal cord, ErbB4 expressed in interneurons regulates mechanical hyperalgesia through the modulation of glycinergic inhibition [37]. Together with these observations, our findings support the concept that ErbB4 functions as a potential neuronal mechanosensor for

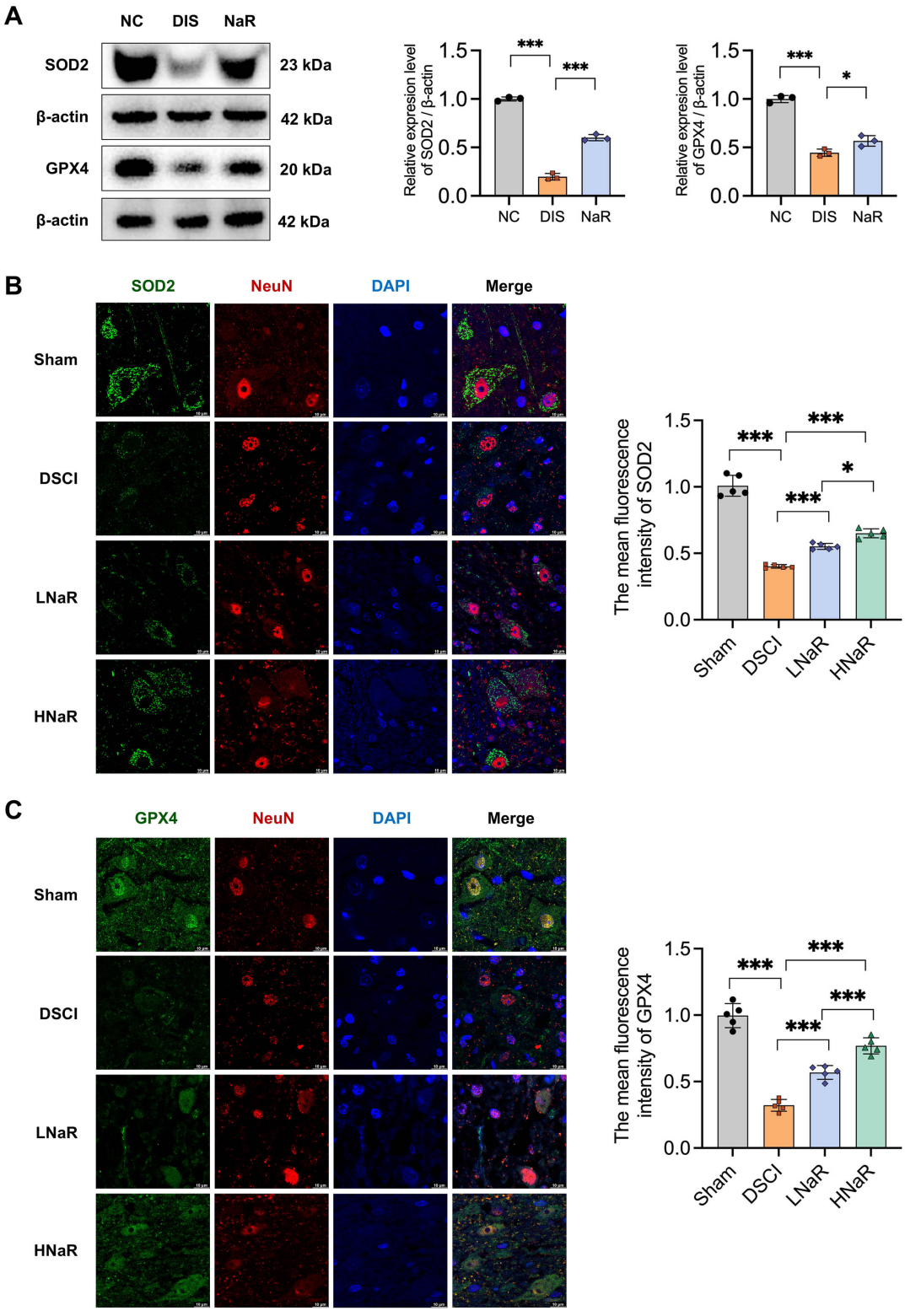

Fig. 6. NaR attenuates mitochondrial oxidative stress by upregulating SOD2 and GPX4. (A) Western blot analysis and quantification of SOD2 and GPX4 expression in SH-SY5Y cells from the NC, DIS, and NaR-treated groups (n = 3). (B,C) Immunofluorescence analysis and quantification of SOD2 (green, B) and GPX4 (green, C) in the neurons (NeuN, red) of spinal cord tissues, respectively (n = 5). NeuN is shown in red, and nuclei are counterstained with DAPI (blue). Scale bar = 10 μm. Data are presented as mean ± SD. *$p < 0.05$, ***$p < 0.001$ for comparisons between groups. SOD2, superoxide dismutase 2; GPX4, glutathione peroxidase 4.

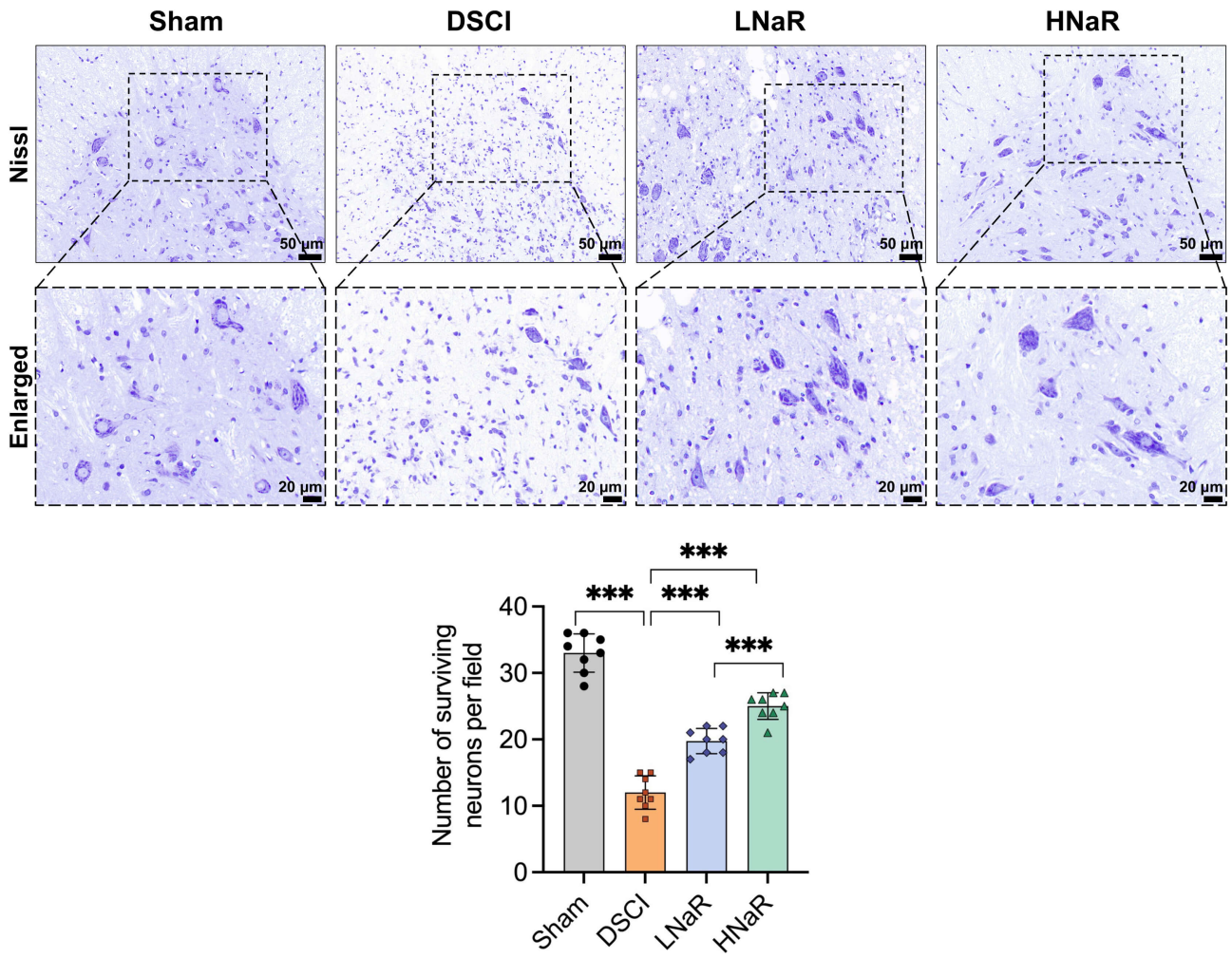

Fig. 7. NaR increases the number of surviving neurons 28 days post-DSCI. Representative images of Nissl-stained sections and quantitative analysis of Nissl-positive motor neurons in the anterior horn of the spinal cord (n = 8). Counts were performed per 200× magnification fields. Scale bars = 20 or 50 μm. Data are presented as mean ± SD. ***$p < 0.001$ for comparisons between groups.

DSCI. We propose that suppression of ErbB4/Akt signaling represents a key event linking sustained mechanical DIS to mitochondrial dysfunction and apoptotic activation, and that restoration of this pathway by NaR limits neuronal loss and facilitates functional recovery after DSCI.

Oxidative stress is a major driver of neuronal apoptosis, with mitochondria serving as central regulators of ROS homeostasis [17]. Within the mitochondrial matrix, SOD2 converts superoxide anions to hydrogen peroxide, which is subsequently detoxified by GPX4, forming a coordinated antioxidant defense system [19]. However, the role of NaR in regulating mitochondrial oxidative stress and apoptosis following DSCI remains unclear. In this study, a marked increase in mitochondrial ROS and loss of MMP are key events that may promote neuronal apoptosis after DSCI. Mitochondria-dependent apoptosis has been linked to excessive activation of ROS-driven mitochondrial fission pathways, which amplify oxidative stress and cellular injury [41]. Moreover, it has been reported that elevated ROS can trigger apoptotic signaling cascades that promote Caspase-3 cleavage, further exacerbating neuronal apoptosis [42]. As depicted in Fig. 8, this represents the critical pathway through which ROS-Caspase-3 signaling mediates neuronal apoptosis post-DSCI. Decline in MMP represents a critical step in the mitochondrial apoptotic cascade; early MMP depolarization reflects an irreversible commitment to apoptosis [43]. Bax/Bak-mediated mitochondrial outer membrane permeabilization leads to cytochrome c release and activation of the caspase cascade, ultimately resulting in programmed cell death [1].

Our findings indicate that NaR disrupts this pathological cycle of oxidative stress and mitochondrial dysfunction. NaR reduced mitochondrial ROS accumulation and preserved MMP, consistent with the enhanced expression of antioxidant enzymes such as SOD2 and GPX4. These effects were accompanied by suppression of the intrinsic

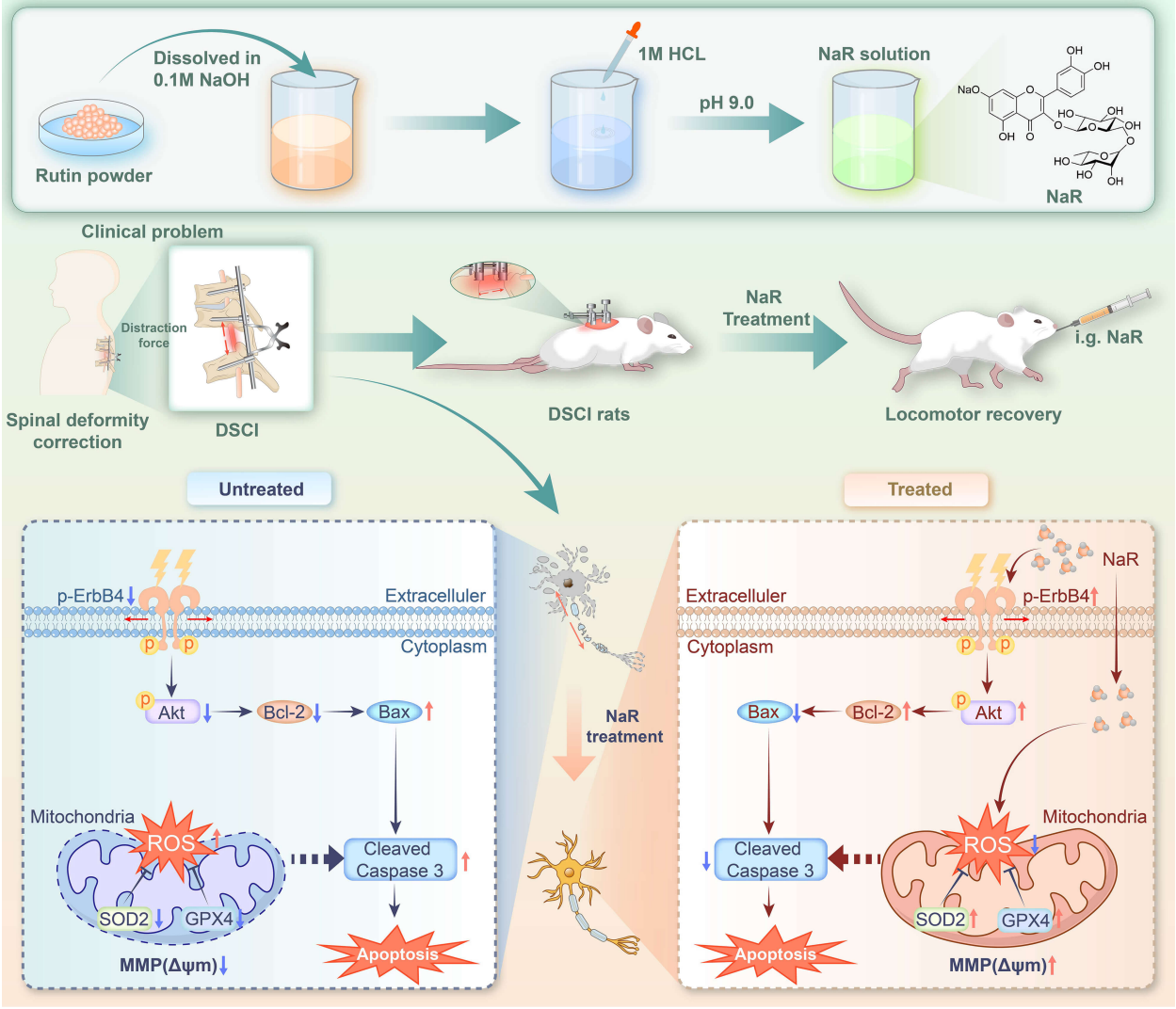

Fig. 8. Schematic overview of NaR preparation and its neuroprotective mechanism in DSCI. The upper panel illustrates the preparation process of NaR from rutin, as previously reported, along with the chemical structure of NaR. The lower panels depict the experimental model and proposed mechanism. In DSCI, reduced ErbB4 phosphorylation suppresses Akt signaling, and activates the Bcl-2/Bax/Caspase-3 apoptotic pathway; simultaneously, mechanical DIS increases mitochondrial ROS levels and attenuates the mitochondrial membrane potential, ultimately leading to neuronal loss and impaired locomotor function. NaR treatment restores ErbB4/Akt pathway phosphorylation, reduces mitochondrial oxidative stress by increasing SOD2 and GPX4 expression, preserves mitochondrial function, and suppresses apoptosis in damaged neurons. These effects are associated with improved tissue integrity and locomotor recovery after DSCI. In the cell pathway mechanism panel, orange upward arrows (to the right of proteins, ROS, and MMP/ΔΨm) indicate upregulation, blue downward arrows indicate downregulation, and other arrows denote the direction of signal transduction or drug action. i.g., intragastric gavage.

apoptotic pathway, including restoration of Bcl-2 levels and reduction of Bax and cleaved Caspase-3 expression. The Bcl-2/Bax/Caspase-3 signaling axis is a well-established mediator of neuronal apoptosis in SCI [44], and modulation of this pathway by NaR aligns with the reported antioxidant and cytoprotective properties of flavonoids such as rutin [45]. Crucially, the anti-apoptotic effects of NaR mediated via the Bcl-2/Bax/Caspase-3 cascade were significantly reversed by the ErbB4 inhibitor Dac, underscoring the ErbB4/Akt axis as the pivotal upstream regulatory pathway. Collectively, these findings demonstrate that following DSCI, impaired ErbB4/Akt-mediated survival signaling—compounded by mitochondrial ROS accumulation and the loss of MMP—converges to drive neuronal apoptosis. Conversely, NaR treatment counteracts this pathological cascade by reactivating the protective ErbB4/Akt pathway while restoring redox homeostasis and preserving mitochondrial function, ultimately attenuating neuronal death.

From a translational perspective, the neuroprotective effects of NaR in DSCI are associated with the restoration of ErbB4 and ROS signaling and improved locomotor outcomes. Compared with its parent compound rutin, NaR exhibits improved solubility, bioavailability, and barrier permeability, enabling effective accumulation at spinal lesion sites, which is consistent with our prior results [9,10]. These findings position NaR as a pharmacological candidate capable of targeting mechanosensitive injury pathways in DSCI and highlight ErbB4/Akt signaling and ROS signaling as a potential therapeutic axis for mitigating DIS-induced neurological deficits. Future work should focus on elucidating the pharmacokinetic profile of NaR and evaluating its efficacy in non-human primate models of DSCI, with the ultimate aim of assessing its potential for clinical translation.

Although this study provides novel insights into the mechanisms of neuronal death following DSCI and proposes a potential therapeutic strategy, it has several limitations. First, our investigation primarily focused on apoptosis, which is the most common form of neuronal death post-SCI. Whether other modalities of cell death concurrently contribute to neuronal loss in the context of DSCI requires further exploration. Second, although we demonstrated that NaR treatment effectively attenuates mitochondrial ROS overproduction, whether a regulatory relationship exists between ErbB4 and ROS signaling remains to be fully elucidated. Future studies employing specific gene knockdown or overexpression approaches are required to definitively validate this signaling axis.

5. Conclusions

In summary, this study identified the ErbB4 and ROS signaling axis as a mechanosensitive pathway regulating neuronal survival during sustained spinal DIS. Mechanical DIS reduced ErbB4 phosphorylation, suppressed Akt signaling, and promoted mitochondrial oxidative stress and activation of the Bcl-2/Bax/Caspase-3 apoptotic cascade. NaR counteracted these effects by restoring ErbB4 signaling, improving mitochondrial redox balance and MMP, and alleviating neuronal apoptosis. These molecular effects were accompanied by improved tissue preservation and locomotor recovery in a rat model of DSCI. Given its improved solubility and bioavailability relative to the parent compound, NaR represents a potential pharmacological strategy for reducing neurological complications associated with spinal deformity correction and highlights ErbB4 and ROS signaling as candidate therapeutic targets in DSCI.

Availability of Data and Materials

The data during the research are available from the corresponding authors on reasonable request.

Author Contributions

YH and WSL conceived the project. WSL, YQX, JJH, DS, YHY, CW, PY and BH performed the experiments and statistical analysis. YJL synthesized sodium rutin. YH, XJQ, WSL and YQX analysed the experimental results. WSL and YQX wrote the original draft, which was edited by YH and XJQ. All authors contributed to editorial changes in the manuscript. All authors read and approved the final manuscript. All authors have participated sufficiently in the work and agreed to be accountable for all aspects of the work.

Ethics Approval and Consent to Participate

All animal procedures were performed strictly in accordance with the National Institutes of Health Guide for the Care and Use of Laboratory Animals (8th Edition, National Academies Press, 2011) and approved by the Animal Welfare Committee of Beijing Chaoyang Hospital, Capital Medical University (Approval No. 24-1002).

Acknowledgment

We gratefully acknowledge the support from Joint Laboratory for Research & Treatment of Spinal Cord Injury in Spinal Deformity, Capital Medical University.

Funding

This study was supported by the National Natural Science Foundation of China (No. 82472534) and Beijing Natural Science Foundation (No. L2510029), and National Natural Science Foundation of China (No. 82502979).

Conflicts of Interest

The authors declare no conflicts of interest.

Supplementary Material

Supplementary material associated with this article can be found, in the online version, at https://doi.org/10.31083/JIN51000.

References

[1] Han B, Liang W, Hai Y, Sun D, Ding H, Yang Y, et al. Neurophysiological, histological, and behavioral characterization of animal models of distraction spinal cord injury: a systematic review. Neural Regeneration Research. 2024; 19: 563–570. https://doi.org/10.4103/1673-5374.380871

[2] Man YW, Lui JYS, Lam CY, Cheung JPY, Cheung PWH. Prevalence and Risk Factors for Postoperative Neurological Complications in Spinal Deformity Surgery: A Systematic Review and Proportional Meta-Analysis. Neurospine. 2025; 22: 243–263. https://doi.org/10.14245/ns.2449364.682

[3] Liang W, Han B, Hai Y, Liu Y, Liu X, Yang J, et al. The Role of Microglia/Macrophages Activation and TLR4/NF-κB/MAPK Pathway in Distraction Spinal Cord Injury-Induced Inflammation. Frontiers in Cellular Neuroscience. 2022; 16: 926453. https://doi.org/10.3389/fncel.2022.926453

[4] Chen W, Gao X, Yang W, Xiao X, Pan X, Li H. Htr2b Pro-

motes M1 Microglia Polarization and Neuroinflammation after Spinal Cord Injury via Inhibition of Neuregulin-1/ErbB Signaling. Molecular Neurobiology. 2024; 61: 1643–1654. https://doi.org/10.1007/s12035-023-03656-6

[5] Cui Y, Bai M, Gao S, Zhao H, Mei X. Zinc ions facilitate metabolic bioenergetic recovery post spinal cord injury by activating microglial mitophagy through the STAT3-FOXO3a-SOD2 pathway. Free Radical Biology & Medicine. 2025; 227: 64–79. https://doi.org/10.1016/j.freeradbiomed.2024.11.045

[6] Chen B, Hu R, Wu X, Shi M, Chen Y, Zhang J, et al. Electroacupuncture Modulation of Chondroitin Sulfate Glycosaminoglycan Promotes the Repair of Damaged Spinal Cord in Rats. Journal of Integrative Neuroscience. 2026; 25: 46448. https://doi.org/10.31083/JIN46448

[7] Forouzanfar F, Sahranavard T, Tsatsakis A, Iranshahi M, Rezaee R. Rutin: a pain-relieving flavonoid. Inflammopharmacology. 2025; 33: 1289–1301. https://doi.org/10.1007/s10787-025-01671-8

[8] Hai JJ, Liang W, Sun D, Yin P, Han B, Qu X. Rutin Attenuates Distraction Spinal Cord Injury by Inhibiting Microglial Inflammation Through Downregulation of P38 MAPK/NF-κB/STAT3 Pathway. Molecular Neurobiology. 2025; 62: 6027–6040. https://doi.org/10.1007/s12035-024-04659-7

[9] Li S, Li J, Pan R, Cheng J, Cui Q, Chen J, et al. Sodium rutin extends lifespan and health span in mice including positive impacts on liver health. British Journal of Pharmacology. 2022; 179: 1825–1838. https://doi.org/10.1111/bph.15410

[10] Pan RY, Ma J, Kong XX, Wang XF, Li SS, Qi XL, et al. Sodium rutin ameliorates Alzheimer's disease-like pathology by enhancing microglial amyloid-β clearance. Science Advances. 2019; 5: eaau6328. https://doi.org/10.1126/sciadv.aau6328

[11] Cui W, Shen C, Xiong WC, Mei L. Prefrontal ErbB4-positive interneurons for avoidance. Cell Reports. 2025; 44: 115628. https://doi.org/10.1016/j.celrep.2025.115628

[12] Zhang Y, Zhu Y, Wang J, Jin L, Guo M, Chen L, et al. Neuregulin4 Acts on Hypothalamic ErBb4 to Excite Oxytocin Neurons and Preserve Metabolic Homeostasis. Advanced Science (Weinheim, Baden-Wurttemberg, Germany). 2023; 10: e2204824. https://doi.org/10.1002/advs.202204824

[13] Liu C, Zhao Y, Zhang W, Dao JJ, Li Q, Huang J, et al. Targeted activation of ErbB4 receptor ameliorates neuronal deficits and neuroinflammation in a food-borne polystyrene microplastic exposed mouse model. Journal of Neuroinflammation. 2025; 22: 86. https://doi.org/10.1186/s12974-025-03406-6

[14] Chen J, Wang B, Fan D, Chen X, Gao L, Luo Y, et al. Macrophages-derived NRG-1 promotes angiogenesis after ischemic stroke via the Akt-mTOR pathway. Neural Regeneration Research. 2026; 21: 3007–3016. https://doi.org/10.4103/NRR.NRR-D-24-01323

[15] Zhu Z, Shen Q, Zhu L, Wei X. Identification of pivotal genes and pathways for spinal cord injury via bioinformatics analysis. Molecular Medicine Reports. 2017; 16: 3929–3937. https://doi.org/10.3892/mmr.2017.7060

[16] Hua KY, Liu YJ, Ke Q, Song Q, Zhang S, Zhao WJ. Downregulation of neuregulin2 (NRG2) following spinal cord injury in C57BL/6 mice: Its implications in therapeutic potential. Iranian Journal of Basic Medical Sciences. 2025; 28: 1075–1081. https://doi.org/10.22038/ijbms.2025.83787.18131

[17] Wang J, Li R, Qian L. Intercellular mitochondrial transfer rewires redox signaling and metabolic plasticity: mechanisms, disease relevance and therapeutic frontiers. Redox Biology. 2026; 90: 104019. https://doi.org/10.1016/j.redox.2026.104019

[18] Li Q, Hong H, Xu G, Xia M, Wang T, Zhou Z, et al. Poliumoside Alleviates Neuroinflammation and Oxidative Stress After Spinal Cord Injury by Activating the PI3K/AKT/mTOR Signaling Pathway. Journal of Integrative Neuroscience. 2025; 24: 43900. https://doi.org/10.31083/JIN43900

[19] Alves F, Lane D, Nguyen TPM, Bush AI, Ayton S. In defence of ferroptosis. Signal Transduction and Targeted Therapy. 2025; 10: 2. https://doi.org/10.1038/s41392-024-02088-5

[20] Hu S, Fei Y, Jin C, Yao J, Ding H, Wang J, et al. Ginsenoside Rd enhances blood-brain barrier integrity after cerebral ischemia/reperfusion by alleviating endothelial cells ferroptosis via activation of NRG1/ErbB4-mediated PI3K/Akt/mTOR signaling pathway. Neuropharmacology. 2024; 251: 109929. https://doi.org/10.1016/j.neuropharm.2024.109929

[21] Hemphill MA, Dabiri BE, Gabriele S, Kerscher L, Franck C, Goss JA, et al. A possible role for integrin signaling in diffuse axonal injury. PloS One. 2011; 6: e22899. https://doi.org/10.1371/journal.pone.0022899

[22] Miao Y, Zhang Y, Zhang L, Chen H, Tang L, Li W, et al. Vitamin D ameliorates prediabetic cardiac injure via modulation of the ErbB4/ferroptosis signaling axis. Frontiers in Immunology. 2025; 16: 1626295. https://doi.org/10.3389/fimmu.2025.1626295

[23] Basso DM, Beattie MS, Bresnahan JC. A sensitive and reliable locomotor rating scale for open field testing in rats. Journal of Neurotrauma. 1995; 12: 1–21. https://doi.org/10.1089/neu.1995.12.1

[24] Liu X, Zhou Y, Wang Z, Yang J, Gao C, Su Q. Effect of VEGF and CX43 on the promotion of neurological recovery by hyperbaric oxygen treatment in spinal cord-injured rats. The Spine Journal : Official Journal of the North American Spine Society. 2014; 14: 119–127. https://doi.org/10.1016/j.spinee.2013.06.084

[25] Xu Y, Geng Y, Wang H, Zhang H, Qi J, Li F, et al. Cyclic helix B peptide alleviates proinflammatory cell death and improves functional recovery after traumatic spinal cord injury. Redox Biology. 2023; 64: 102767. https://doi.org/10.1016/j.redox.2023.102767

[26] Chen S, Ye J, Chen X, Shi J, Wu W, Lin W, et al. Valproic acid attenuates traumatic spinal cord injury-induced inflammation via STAT1 and NF-κB pathway dependent of HDAC3. Journal of Neuroinflammation. 2018; 15: 150. https://doi.org/10.1186/s12974-018-1193-6

[27] Li Z, Yang X, Mao J, Zeng P, Qi Y, Shi Y, et al. Senecavirus a VP2 protein orchestrates PRDX1 degradation through dual autophagy pathways: macroautophagy and chaperone-mediated autophagy. Autophagy. 2026; 22: 744–762. https://doi.org/10.1080/15548627.2025.2610449

[28] Qian D, Xu J, Zhang X, Hu F, Cao S, Dong Y, et al. Microenvironment Self-Adaptive Nanomedicine Promotes Spinal Cord Repair by Suppressing Inflammation Cascade and Neural Apoptosis. Advanced Materials (Deerfield Beach, Fla.). 2024; 36: e2307624. https://doi.org/10.1002/adma.202307624

[29] Li C, Wu Z, Zhou L, Shao J, Hu X, Xu W, et al. Temporal and spatial cellular and molecular pathological alterations with single-cell resolution in the adult spinal cord after injury. Signal Transduction and Targeted Therapy. 2022; 7: 65. https://doi.org/10.1038/s41392-022-00885-4

[30] Ma Y, Ju C, Yu X, Zhao Y, Liu S, Li H, et al. Multifunctional Diselenide-Based Antioxidative Nanozymes Promote Spinal Cord Repair via Oxidative Stress Alleviation and Immune Modulation. ACS Nano. 2026; 20: 4116–4142. https://doi.org/10.1021/acsnano.5c15784

[31] Li X, Li W, Xie X, Fang T, Yang J, Shen Y, et al. ROS Regulate Rotenone-induced SH-SY5Y Dopamine Neuron Death Through Ferroptosis-mediated Autophagy and Apoptosis. Molecular Neurobiology. 2025; 62: 9271–9289. https://doi.org/10.1007/s12035-025-04824-6

[32] Khuyagbaatar B, Kim K, Man Park W, Hyuk Kim Y. Biomechanical Behaviors in Three Types of Spinal Cord Injury Mech-

anisms. Journal of Biomechanical Engineering. 2016; 138: 081003. https://doi.org/10.1115/1.4033794

[33] Chen K, Liu J, Assinck P, Bhatnagar T, Streijger F, Zhu Q, et al. Differential Histopathological and Behavioral Outcomes Eight Weeks after Rat Spinal Cord Injury by Contusion, Dislocation, and Distraction Mechanisms. Journal of Neurotrauma. 2016; 33: 1667–1684. https://doi.org/10.1089/neu.2015.4218

[34] Han C, Hai Y, Yin P, Cha T, Li G. In vivo deformation of the spine canal before and after surgical corrections of severe and rigid kyphoscoliosis. Journal of Orthopaedic Translation. 2020; 23: 1–7. https://doi.org/10.1016/j.jot.2020.03.009

[35] Yin P, Liang W, Han B, Yang Y, Sun D, Qu X, et al. Hydrogel and Nanomedicine-Based Multimodal Therapeutic Strategies for Spinal Cord Injury. Small Methods. 2024; 8: e2301173. https://doi.org/10.1002/smtd.202301173

[36] Rojas A, Dahlen S, Zhang F, Liu S. The Cytoskeletal Structure in Cardiomyocyte Maturation and Proliferation. Cells. 2025; 14: 1494. https://doi.org/10.3390/cells14191494

[37] Yu Y, Wei G, Zhou Q, Sha H. ErbB4 in Spinal PV Interneurons Regulates Mechanical Allodynia in Neuropathic Pain via Modulation of Glycinergic Inhibitory Tone. Journal of Pain Research. 2021; 14: 1643–1651. https://doi.org/10.2147/JPR.S311894

[38] Schlessinger J, Lemmon MA. Nuclear signaling by receptor tyrosine kinases: the first robin of spring. Cell. 2006; 127: 45–48. https://doi.org/10.1016/j.cell.2006.09.013

[39] Nawwar DA, Zaki HF, Sayed RH. Role of the NRG1/ErbB4 and PI3K/AKT/mTOR signaling pathways in the anti-psychotic effects of aripiprazole and sertindole in ketamine-induced schizophrenia-like behaviors in rats. Inflammopharmacology. 2022; 30: 1891–1907. https://doi.org/10.1007/s10787-022-01031-w

[40] Haskins JW, Nguyen DX, Stern DF. Neuregulin 1-activated ERBB4 interacts with YAP to induce Hippo pathway target genes and promote cell migration. Science Signaling. 2014; 7: ra116. https://doi.org/10.1126/scisignal.2005770

[41] Chang X, Niu S, Shang M, Li J, Guo M, Zhang W, et al. ROS-Drp1-mediated mitochondria fission contributes to hippocampal HT22 cell apoptosis induced by silver nanoparticles. Redox Biology. 2023; 63: 102739. https://doi.org/10.1016/j.redox.2023.102739

[42] Tang S, Yu X, Zhang L, Bu X, Wang W, Xia Z. KIF23 inhibition protects against perioperative neurocognitive disorders by hindering ROS/caspase-3/GSDME-mediated pyroptosis. Experimental Neurology. 2025; 393: 115371. https://doi.org/10.1016/j.expneurol.2025.115371

[43] Awad-Igbaria Y, Ben-Menashe A, Sakas R, Edelman D, Fishboom T, Shamir A, et al. Novel insight into TRPV1-induced mitochondrial dysfunction in neuropathic pain. Brain : a Journal of Neurology. 2025; 148: 2563–2578. https://doi.org/10.1093/brain/awaf044

[44] Han B, Liang W, Hai Y, Liu Y, Chen Y, Ding H, et al. Elucidating the Potential Mechanisms Underlying Distraction Spinal Cord Injury-Associated Neuroinflammation and Apoptosis. Frontiers in Cell and Developmental Biology. 2022; 10: 839313. https://doi.org/10.3389/fcell.2022.839313

[45] Lai X, Zhang Y, Wu J, Shen M, Yin S, Yan J. Rutin Attenuates Oxidative Stress Via PHB2-Mediated Mitophagy in MPP^+-Induced SH-SY5Y Cells. Neurotoxicity Research. 2023; 41: 242–255. https://doi.org/10.1007/s12640-023-00636-5